This document is downloaded from DR-NTU (https://dr.ntu.edu.sg)
Nanyang Technological University, Singapore.

High-performance GeSn photodetector and fin field-effect transistor (FinFET) on an advanced GeSn-on-insulator platform

Wang, Wei; Lei, Dian; Huang, Yi-Chiau; Lee, Kwang Hong; Loke, Wan-Khai; Dong, Yuan; Xu, Shengqiang; Tan, Chuan Seng; Wang, Hong; Yoon, Soon-Fatt; Gong, Xiao; Yeo, Yee-Chia

2018

Wang, W., Lei, D., Huang, Y.-C., Lee, K. H., Loke, W.-K., Dong, Y., . . . Yeo, Y.-C. (2018). High-performance GeSn photodetector and fin field-effect transistor (FinFET) on an advanced GeSn-on-insulator platform. Optics Express, 26(8), 10305-.

https://hdl.handle.net/10356/83638

https://doi.org/10.1364/OE.26.010305

© 2018 Optical Society of America under the terms of the OSA Open Access Publishing Agreement. Users may use, reuse, and build upon the article, or use the article for text or data mining, so long as such uses are for non-commercial purposes and appropriate attribution is maintained. All other rights are reserved.

Downloaded on 28 Aug 2022 01:01:23 SGT

Research Article | Vol. 26, No. 8 | 16 Apr 2018 | OPTICS EXPRESS 10305

Optics EXPRESS

High-performance GeSn photodetector and fin field-effect transistor (FinFET) on an advanced GeSn-on-insulator platform

WEI WANG,[1] DIAN LEI,[1] YI-CHIAU HUANG,[2] KWANG HONG LEE,[3] WAN-KHAI LOKE,[4] YUAN DONG,[1] SHENGQIANG XU,[1] CHUAN SENG TAN,[3,4] HONG WANG,[4] SOON-FATT YOON,[4] XIAO GONG,[1,5] AND YEE-CHIA YEO[1,6]

[1]*Department of Electrical and Computer Engineering, National University of Singapore, 117576 Singapore*
[2]*Applied Materials Inc., Sunnyvale, California, USA*
[3]*Low Energy Electronic Systems (LEES), Singapore MIT Alliance for Research and Technology (SMART), Singapore*
[4]*School of Electrical and Electronic Engineering, Nanyang Technological University, 639798 Singapore*
[5]*elegong@nus.edu.sg*
[6]*eleyeoyc@nus.edu.sg*

Abstract: We report the first demonstration of high-performance GeSn metal-semiconductor-metal (MSM) photodetector and GeSn p-type fin field-effect transistor (pFinFET) on an advanced GeSn-on-insulator (GeSnOI) platform by complementary metal-oxide-semiconductor (CMOS) compatible processes. The detection range of GeSn photodetector is extended beyond 2 µm, with responsivities of 0.39 and 0.10 A/W at 1550 nm and 2003 nm, respectively. Through the insertion of an ultrathin Al_2O_3 Schottky-barrier-enhancement layer, the dark current I_{Dark} of the GeSn photodetector is suppressed by more than 2 orders of magnitude. An impressive I_{Dark} of ~65 nA was achieved at an operating voltage of 1.0 V. A frequency response measurement reveals the achievement of a 3-dB bandwidth of ~1.4 GHz at an illumination wavelength of 2 µm. GeSn pFinFET with fin width (W_{fin}) scaled down to 15 nm was also fabricated on the GeSnOI platform, exhibiting a small subthreshold swing (S) of 93 mV/decade, a high drive current of 176 µA/µm, and good control of short channel effects (SCEs). This work paves the way for realizing compact, low-cost, and multi-functional GeSn-on-insulator opto-electronic integrated circuits.

© 2018 Optical Society of America under the terms of the OSA Open Access Publishing Agreement

OCIS codes: (250.0250) Optoelectronics; (130.0130) Integrated optics; (230.5170) Photodiodes; (040.3060) Infrared.

References and links

1. G. H. Gelinck, H. E. A. Huitema, E. van Veenendaal, E. Cantatore, L. Schrijnemakers, J. B. van der Putten, T. C. Geuns, M. Beenhakkers, J. B. Giesbers, B. H. Huisman, E. J. Meijer, E. M. Benito, F. J. Touwslager, A. W. Marsman, B. J. van Rens, and D. M. de Leeuw, "Flexible active-matrix displays and shift registers based on solution-processed organic transistors," Nat. Mater. **3**(2), 106–110 (2004).
2. S. Xu, Y. Zhang, L. Jia, K. E. Mathewson, K. I. Jang, J. Kim, H. Fu, X. Huang, P. Chava, R. Wang, S. Bhole, L. Wang, Y. J. Na, Y. Guan, M. Flavin, Z. Han, Y. Huang, and J. A. Rogers, "Soft microfluidic assemblies of sensors, circuits, and radios for the skin," Science **344**(6179), 70–74 (2014).
3. W. Wu, X. Wen, and Z. L. Wang, "Taxel-addressable matrix of vertical-nanowire piezotronic transistors for active and adaptive tactile imaging," Science **340**(6135), 952–957 (2013).
4. J. D. Gallagher, C. L. Senaratne, J. Kouvetakis, and J. Menendez, "Compositional dependence of the bowing parameter for the direct and indirect band gaps in $Ge_{1-y}Sn_y$ alloys," Appl. Phys. Lett. **105**(14), 142102 (2014).
5. R. Chen, H. Lin, Y. Huo, C. Hitzman, T. I. Kamins, and J. S. Harris, "Increased photoluminescence of strain-reduced, high-Sn composition $Ge_{1-x}Sn_x$ alloys grown by molecular beam epitaxy," Appl. Phys. Lett. **99**(18), 181125 (2011).
6. A. A. Tonkikh, C. Eisenschmidt, V. G. Talalaev, N. D. Zakharov, J. Schilling, G. Schmidt, and P. Werner, "Pseudomorphic GeSn/Ge(001) quantum wells: examining indirect band gap bowing," Appl. Phys. Lett. **103**(3), 032106 (2013).

#315805 https://doi.org/10.1364/OE.26.010305
Journal © 2018 Received 18 Dec 2017; revised 25 Mar 2018; accepted 26 Mar 2018; published 10 Apr 2018

7. D. Stange, N. von den Driesch, D. Rainko, S. Roesgaard, I. Povstugar, J. M. Hartmann, T. Stoica, Z. Ikonic, S. Mantl, D. Grützmacher, and D. Buca, "Short-wave infrared LEDs from GeSn/SiGeSn multiple quantum wells," Optica **4**(2), 185–188 (2017).
8. X. Gong, G. Han, F. Bai, S. Su, P. Guo, Y. Yang, R. Cheng, D. Zhang, G. Zhang, C. Xue, B. Cheng, J. Pan, Z. Zhang, E. S. Tok, D. Antoniadis, and Y. C. Yeo, "Germanium-tin (GeSn) p-channel MOSFETs fabricated on (100) and (111) surface orientations with sub-400 °C Si_2H_6 passivation," IEEE Electron Device Lett. **34**(3), 339–341 (2013).
9. S. Gupta, B. Vincent, D. H. C. Lin, M. Gunji, A. Firrincieli, F. Gencarelli, B. Magyari-Köpe, B. Yang, B. Douhard, J. Delmotte, A. Franquet, M. Caymax, J. Dekoster, Y. Nishi, and K. C. Saraswat, "GeSn channel nMOSFETs: material potential and technological outlook," in *Proceedings of IEEE Symposium on VLSI Technology* (IEEE, 2012), pp. 95–96.
10. M. Liu, G. Han, Y. Liu, C. Zhang, H. Wang, X. Li, J. Zhang, B. Cheng, and Y. Hao, "Undoped $Ge_{0.92}Sn_{0.08}$ quantum well PMOSFETs on (001),(011) and (111) substrates with in situ Si_2H_6 passivation: High hole mobility and dependence of performance on orientation," in *Proceedings of IEEE Symposium on VLSI Technology* (IEEE, 2014), pp. 100–101.
11. Y. Liu, J. Yan, H. Wang, Q. Zhang, M. Liu, B. Zhao, C. Zhang, B. Cheng, Y. Hao, and G. Han, "Strained GeSn p-channel metal–oxide–semiconductor field-effect transistors with in situ Si_2H_6 surface passivation: impact of Sn composition," IEEE Trans. Electron Dev. **61**(11), 3639–3645 (2014).
12. D. Lei, W. Wang, Z. Zhang, J. Pan, X. Gong, G. Liang, E.-S. Tok, and Y.-C. Yeo, "$Ge_{0.83}Sn_{0.17}$ p-channel metal-oxide-semiconductor field-effect transistors: impact of sulfur passivation on gate stack quality," J. Appl. Phys. **119**(2), 024502 (2016).
13. Y. S. Huang, C. H. Huang, F. L. Lu, C. Y. Lin, H. Y. Ye, I. H. Wong, S. R. Jan, H. S. Lan, C. W. Liu, Y. C. Huang, H. Chung, C. P. Chang, S. S. Chu, and S. Kuppurao, "Record high mobility ($428cm^2/V$-s) of CVD-grown Ge/strained $Ge_{0.91}Sn_{0.09}$/Ge quantum well p-MOSFETs," in *Proceedings of IEEE International Electron Devices Meeting* (IEEE, 2016), pp. 822–825.
14. G. Han, Y. Wang, Y. Liu, C. Zhang, Q. Feng, M. Liu, S. Zhao, B. Cheng, J. Zhang, and Y. Hao, "GeSn quantum well p-channel tunneling FETs fabricated on Si (001) and (111) with improved subthreshold swing," IEEE Electron Device Lett. **37**(6), 701–704 (2016).
15. Q. Zhang, Y. Liu, J. Yan, C. Zhang, Y. Hao, and G. Han, "Theoretical investigation of tensile strained GeSn waveguide with Si_3N_4 liner stressor for mid-infrared detector and modulator applications," Opt. Express **23**(6), 7924–7932 (2015).
16. Q. Zhang, Y. Liu, J. Yan, C. Zhang, Y. Hao, and G. Han, "Simulation investigation of tensile strained GeSn fin photodetector with Si_3N_4 liner stressor for extension of absorption wavelength," Opt. Express **23**(2), 739–746 (2015).
17. S. Su, B. Cheng, C. Xue, W. Wang, Q. Cao, H. Xue, W. Hu, G. Zhang, Y. Zuo, and Q. Wang, "GeSn p-i-n photodetector for all telecommunication bands detection," Opt. Express **19**(7), 6400–6405 (2011).
18. C. Chang, H. Li, C. T. Ku, S. G. Yang, H. H. Cheng, J. Hendrickson, R. A. Soref, and G. Sun, "$Ge_{0.975}Sn_{0.025}$ 320×256 imager chip for 1.6-1.9 μm infrared vision," Appl. Opt. **55**(36), 10170–10173 (2016).
19. M. P. Hansen and D. S. Malchow, "Overview of SWIR detectors, cameras, and applications," Proc. SPIE **6939**, 69390I (2008).
20. K. Toko, N. Oya, N. Saitoh, N. Yoshizawa, and T. Suemasu, "70° C synthesis of high-Sn content (25%) GeSn on insulator by Sn-induced crystallization of amorphous Ge," Appl. Phys. Lett. **106**(8), 082109 (2015).
21. H. Chikita, R. Matsumura, Y. Kai, T. Sadoh, and M. Miyao, "Ultra-high-speed lateral solid phase crystallization of GeSn on insulator combined with Sn-melting-induced seeding," Appl. Phys. Lett. **105**(20), 202112 (2014).
22. M. Kurosawa, N. Taoka, H. Ikenoue, O. Nakatsuka, and S. Zaima, "Large grain growth of Ge-rich $Ge_{1-x}Sn_x$ ($x \approx 0.02$) on insulating surfaces using pulsed laser annealing in flowing water," Appl. Phys. Lett. **104**(6), 061901 (2014).
23. Z. Liu, J. Wen, X. Zhang, C. Li, C. Xue, Y. Zuo, B. Cheng, and Q. Wang, "High hole mobility GeSn on insulator formed by self-organized seeding lateral growth," J. Phys. D Appl. Phys. **48**(44), 445103 (2014).
24. H. Li, J. Brouillet, A. Salas, X. Wang, and J. Liu, "Low temperature growth of high crystallinity GeSn on amorphous layers for advanced optoelectronics," Opt. Mater. Express **3**(9), 1385–1396 (2013).
25. D. Lei, K. H. Lee, S. Bao, W. Wang, B. Wang, X. Gong, C. S. Tan, and Y. C. Yeo, "GeSn-on-insulator substrate formed by direct wafer bonding," Appl. Phys. Lett. **109**(2), 022106 (2016).
26. P. Hashemi, T. Ando, K. Balakrishnan, J. Bruley, S. Engelmann, J. A. Ott, V. Narayanan, D. G. Park, R. T. Mo, and E. Leobandung, "High-mobility high-Ge-content $Si_{1-x}Ge_x$-OI PMOS FinFETs with fins formed using 3D germanium condensation with Ge fraction up to x~0.7, scaled EOT ~8.5 Å and ~10 nm fin width," in *Proceedings of IEEE Symposium on VLSI Technology* (IEEE, 2015), pp. 16–17.
27. J. H. Nam, F. Afshinmanesh, D. Nam, W. S. Jung, T. I. Kamins, M. L. Brongersma, and K. C. Saraswat, "Monolithic integration of germanium-on-insulator p-i-n photodetector on silicon," Opt. Express **23**(12), 15816–15823 (2015).
28. H. Wu, W. Luo, H. Zhou, M. Si, J. Zhang, and P. D. Ye, "First experimental demonstration of Ge 3D FinFET CMOS circuits," in Proceedings of IEEE Symposium on VLSI Technology (IEEE, 2015), pp. 58–59.
29. M. Pu, L. Ottaviano, E. Semenova, and K. Yvind, "Efficient frequency comb generation in AlGaAs-on-insulator," Optica **3**(8), 823–826 (2016).

30. V. Djara, V. Deshpande, E. Uccelli, N. Daix, D. Caimi, C. Rossel, M. Sousa, H. Siegwart, C. Marchiori, J. M. Hartmann, K. T. Shiu, C. W. Weng, M. Krishnan, M. Lofaro, R. Steiner, D. Sadana, D. Lubyshev, A. Liu, L. Czornomaz, and J. Fompeyrine, "An InGaAs on Si platform for CMOS with 200 mm InGaAs-OI substrate, gate-first, replacement gate planar and FinFETs down to 120 nm contact pitch," in Proceedings of IEEE Symposium on VLSI Technology (IEEE, 2015), pp. 176–177.
31. W. Wang, L. Li, Q. Zhou, J. Pan, Z. Zhang, E. S. Tok, and Y. C. Yeo, "Tin surface segregation, desorption, and island formation during post-growth annealing of strained epitaxial $Ge_{1-x}Sn_x$ layer on Ge(001) substrate," Appl. Surf. Sci. **321**, 240–244 (2014).
32. A. Gassenq, F. Gencarelli, J. Van Campenhout, Y. Shimura, R. Loo, G. Narcy, B. Vincent, and G. Roelkens, "GeSn/Ge heterostructure short-wave infrared photodetectors on silicon," Opt. Express **20**(25), 27297–27303 (2012).
33. Z. Liu, H. Cong, F. Yang, C. Li, J. Zheng, C. Xue, Y. Zuo, B. Cheng, and Q. Wang, "Defect-free high Sn-content GeSn on insulator grown by rapid melting growth," Sci. Rep. **6**(1), 38386 (2016).
34. J.-Y. J. Lin, S. Gupta, Y.-C. Huang, Y. Kim, M. Jin, E. Sanchez, R. Chen, K. Balram, D. Miller, J. Harris, and K. Saraswat, "Fabrication of GeSn-on-insulator (GSOI) to enable monolithic 3D co-integration of logic and photonics," in *Proceedings of IEEE Symposium on VLSI Technology* (IEEE, 2013), pp. 32–33.
35. B. R. Conley, A. Mosleh, S. A. Ghetmiri, W. Du, R. A. Soref, G. Sun, J. Margetis, J. Tolle, H. A. Naseem, and S. Q. Yu, "Temperature dependent spectral response and detectivity of GeSn photoconductors on silicon for short wave infrared detection," Opt. Express **22**(13), 15639–15652 (2014).
36. M. Oehme, K. Kostecki, K. Ye, S. Bechler, K. Ulbricht, M. Schmid, M. Kaschel, M. Gollhofer, R. Körner, W. Zhang, E. Kasper, and J. Schulze, "GeSn-on-Si normal incidence photodetectors with bandwidths more than 40 GHz," Opt. Express **22**(1), 839–846 (2014).
37. O. Nakatsuka, N. Tsutsui, Y. Shimura, S. Takeuchi, A. Sakai, and S. Zaima, "Mobility behavior of $Ge_{1-x}Sn_x$ layers grown on silicon-on-insulator substrates," Jpn. J. Appl. Phys. **49**, 04DA10 (2010).
38. T. Nishimura, K. Kita, and A. Toriumi, "Evidence for strong Fermi-level pinning due to metal-induced gap states at metal/germanium interface," Appl. Phys. Lett. **91**(12), 123123 (2007).
39. L. Low, Y. Yang, G. Han, W. Fan, and Y.-C. Yeo, "Electronic band structure and effective mass parameters of $Ge_{1-x}Sn_x$ alloys," J. Appl. Phys. **112**(10), 103715 (2012).
40. L.-H. Laih, T.-C. Chang, Y.-A. Chen, W.-C. Tsay, and J.-W. Hong, "Characteristics of MSM photodetectors with trench electrodes on p-type Si wafer," IEEE Trans. Electron Dev. **45**(9), 2018–2023 (1998).
41. K. W. Ang, S. Y. Zhu, J. Wang, K. T. Chua, M. B. Yu, G. Q. Lo, and D. L. Kwong, "Novel silicon-carbon (Si:C) Schottky barrier enhancement layer for dark-current suppression in Ge-on-SOI MSM photodetectors," IEEE Electron Device Lett. **29**(7), 704–707 (2008).
42. T. Nishimura, K. Kita, and A. Toriumi, "A significant shift of Schottky barrier heights at strongly pinned metal/germanium interface by inserting an ultra-thin insulating film," Appl. Phys. Express **1**(5), 051406 (2008).
43. Y. Dong, W. Wang, S. Xu, D. Lei, X. Gong, X. Guo, H. Wang, S. Y. Lee, W. K. Loke, S. F. Yoon, and Y. C. Yeo, "Two-micron-wavelength germanium-tin photodiodes with low dark current and gigahertz bandwidth," Opt. Express **25**(14), 15818–15827 (2017).
44. M. Morea, C. E. Brendel, K. Zang, J. Suh, C. S. Fenrich, Y.-C. Huang, H. Chung, Y. Huo, T. I. Kamins, K. C. Saraswat, and J. S. Harris, "Passivation of multiple-quantum-well $Ge_{0.97}Sn_{0.03}$/Ge p-i-n photodetectors," Appl. Phys. Lett. **110**(9), 091109 (2017).
45. T. Pham, W. Du, H. Tran, J. Margetis, J. Tolle, G. Sun, R. A. Soref, H. A. Naseem, B. Li, and S.-Q. Yu, "Systematic study of Si-based GeSn photodiodes with 2.6 μm detector cutoff for short-wave infrared detection," Opt. Express **24**(5), 4519–4531 (2016).
46. Y. H. Huang, G. E. Chang, H. Li, and H. H. Cheng, "Sn-based waveguide p-i-n photodetector with strained GeSn/Ge multiple-quantum-well active layer," Opt. Lett. **42**(9), 1652–1655 (2017).
47. W. Wang, Y. Dong, S. Y. Lee, W. K. Loke, D. Lei, S. F. Yoon, G. Liang, X. Gong, and Y. C. Yeo, "Floating-base germanium-tin heterojunction phototransistor for high-efficiency photodetection in short-wave infrared range," Opt. Express **25**(16), 18502–18507 (2017).
48. V. R. D'Costa, W. Wang, and Y. C. Yeo, "Near-bandgap optical properties of pseudomorphic GeSn alloys grown by molecular beam epitaxy," J. Appl. Phys. **120**(6), 063104 (2016).
49. K. Thyagarajan and A. Ghatak, *Fiber Optic Essentials* (John Wiley & Sons, 2007).
50. P. C. Hobbs, *Building Electro-optical Systems: Making it all Work* (John Wiley & Sons, 2011).
51. C. Lim and R. A. Moore, "Properties of alternately charged coplanar parallel strips by conformal mapping," IEEE Trans. Electron Dev. **15**(3), 173–180 (1968).

1. Introduction

Stacking of semiconductor and insulator thin films is one of the important approaches used to realize monolithic three-dimensional (3D) integration of circuits, which can raise the degree of complexity of multifunctional circuits that comprise electronic and optoelectronic devices. In addition, the synthesis of semiconductor on insulators enables the integration of semiconductor devices on multi-functional glass displays or on flexible substrates. Integration

on flexible substrates are needed for paper-like devices [1], or bio-integrated devices [2,3] as they require unique features such as wearability and biocompatibility.

The interest in germanium-tin alloy (GeSn or $Ge_{1-x}Sn_x$) has significantly increased recently as it has tunable direct band gap [4–7] and higher hole mobility than those of Si and Ge [8–14]. As a group IV material, high crystalline quality GeSn can be epitaxially grown on Si substrate, making it an ideal material for co-integration of high speed complementary metal-oxide-semiconductor (CMOS) logic and Si-compatible photonics in the short-wave infrared range (SWIR, wavelength λ~1-3 µm) [15–17]. This light spectrum range finds applications in a variety of areas, including chemical and biological sensing, night vision, medical diagnostics, and fiber-optic telecommunications [17–19]. The study of GeSn-on-insulators (GeSnOIs) has been accelerated recently, due to its potential application in 3D integration and in flexible/wearable electronics and optoelectronics. However, most of the research effort has been focused on the formation and characterization of the GeSn film on insulator [20–25]. Unlike the Silicon-Germanium-on-insulator (SGOI) [26], Germanium-on-insulator (GeOI) [27,28], and III-V-on-insulator (III-VOI) [29,30] platforms, where there are many reports on realization of electronic and photonic devices, there are few reports on GeSnOI devices [23], and device performance data on GeSnOI platform is limited.

In this work, both GeSn metal-semiconductor-metal (MSM) photodetector and GeSn p-type fin field-effect transistor (pFinFET) were fabricated separately on a novel GeSnOI platform. The high crystalline quality GeSnOI platform was formed by a direct wafer bonding technique. The entire process flow is CMOS compatible, with the processing temperatures kept below 400 °C in order to prevent Sn segregation or precipitation [31]. The low process temperature enables either "electronic-first and photonic-last" or "photonic-first and electronic-last" integration approach for monolithically fabricating the GeSn photodetector and CMOS integrated circuit. Through insertion of an Al_2O_3 Schottky-barrier-enhancement layer beneath the metal contact, GeSn MSM photodetector with low dark current, high responsivity and gigahertz bandwidth was realized. Besides the high performance GeSn photodetector, GeSn pFinFETs with fin width (W_{fin}) down to 15 nm were also fabricated on GeSnOI platform. Small subthreshold swing (S) of 93 mV/decade, high drive current of 176 µA/µm, and good control of short channel effects (SCEs) were obtained at fin width (W_{fin}) of 15 nm.

2. Device design and fabrication

Figure 1 shows a schematic of a GeSn MSM photodetector and a GeSn FinFET on a GeSnOI platform. This illustration shows a way to monolithically integrate electronic and photonic devices on the same platform. A direct wafer bonding technique was used to form the GeSnOI platform as described in [25]. The donor wafer is a ~100 nm-thick GeSn layer on a ~1 µm-thick Ge buffer grown by chemical vapor deposition (CVD) on a 12-inch Si substrate. After growth, the wafer was cut into 2-inch piece, and bonded to a Si wafer. High-resolution x-ray diffraction reciprocal space mapping shows that the GeSn layer is fully strained to the Ge buffer, with the substitutional Sn composition of ~8.0% and the compressive strain of ~0.9%. After wafer bonding, the backside Si from the donor wafer was selectively etched with respect to the Ge buffer using tetramethylammonium hydroxide (TMAH) solution (25% by weight). The Ge buffer layer was then thinned down using SF_6-based inductively coupled plasma (ICP).

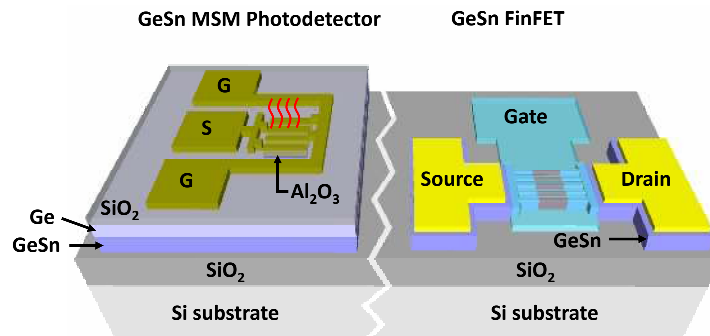

Fig. 1. Schematic of a GeSn MSM photodetector and a MOSFET formed on GeSn-on-insulator platform. This illustration shows a way to monolithically integrate electronic and photonic devices on the same platform.

A MSM photodetector was selected for demonstration due to its ease of process integration (no specific doping profile required), high responsivity (optical gain) and high-speed operation (low capacitance). A ~90-nm-thick Ge layer (top portion of Ge buffer layer) was left on the GeSn surface, i.e. the Ge buffer was not completely removed. After 100-nm-thick SiO_2 deposition, the contact region was opened by dry etching followed by wet etching using 1:50 diluted HF solution. A ~1.5 nm-thick Al_2O_3 layer was then deposition by atomic layer deposition (ALD) at a process temperature of 250 °C. After deposition of ~150 nm Al, a lift-off process completes the fabrication of the finger-type MSM structure. A GeSn MSM photodetector without Al_2O_3 interlayer was also fabricated for comparison. Figure 2(a) shows the top-view SEM image of a GeSn MSM photodetector with a ground-signal-ground (GSG) electrode configuration. The scanning transmission electron microscopy (STEM) image cut across the metal finger shows the defect-free Ge and GeSn layers on SiO_2 [Fig. 2(b)], with thickness of ~90 nm and ~100 nm, respectively. No void was observed at the SiO_2/Si bonding interface, indicating that a seamless bond was achieved. Clear lattice fringes can be observed in Ge and GeSn layers [Fig. 2(c) and 2(d)], with an ultrathin Al_2O_3 layer inserted between Al and Ge.

To control the SCEs and off-state leakage in transistor with extremely scaled dimensions, the multi-gate transistor architecture formed on semiconductor-on-insulator substrate is very attractive. The GeSn pFinFET with fin width (W_{fin}) down to 15 nm was fabricated on the GeSnOI platform. After removing the Ge buffer, the GeSn layer was thinned down to ~35 nm using chemical mechanical polishing (CMP). Smooth GeSnOI sample was formed with a surface root-mean-square roughness of ~0.2 nm. The channel region was then defined by electron beam lithography (EBL). The source/drain (S/D) regions were formed by Boron implantation followed by dopant activation at 400 °C for 60 s. After GeSn fin formation by dry etching, the sample was immediately loaded into an ultra-high vacuum chamber for Si passivation at 370 °C. Gate stack was then formed by deposition of 4 nm-thick HfO_2 using ALD and deposition of Mo/W using Sputter. Gate etch process was performed using F-based plasma etch. Finally, Ni was deposited at the S/D contact region to complete the device fabrication. Tilted-view SEM image in Fig. 2(e) shows a fabricated GeSn pFinFET. XTEM image of a GeSn pFinFET cut across the gate line shows smooth GeSn fin sidewall [Fig. 2(f)], with W_{fin} of ~30 nm and fin height (H_{fin}) of 35 nm. No Sn segregation or precipitation can be observed after device fabrication [Fig. 2(g)].

Optics EXPRESS

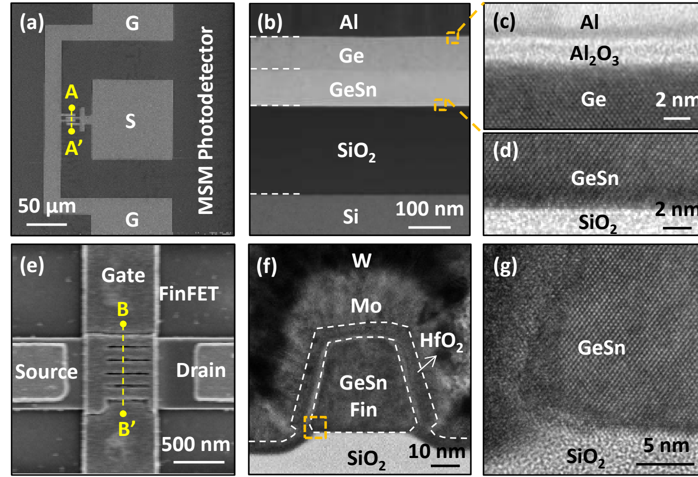

Fig. 2. (a) Top-view SEM and (b) cross-sectional STEM images of a GeSn MSM photodetector cut across the AA'. The GSG contact pads were formed on SiO_2. HRTEM images of (c) $Al/Al_2O_3/Ge$ contact and (d) $GeSn/SiO_2$ interface. Crystalline Ge and GeSn layer were formed on SiO_2. A clear Al_2O_3 interlayer can be observed between Al and Ge. (e) Tilted-view SEM and (f) cross-sectional TEM image of a GeSn FinFET (W_{fin} = 30 nm) cut across the BB'. Well-defined GeSn fin structure can be observed. (g) HRTEM image shows crystalline GeSn fin on SiO_2 with a smooth sidewall.

3. Results and discussion

3.1 Dark current reduction in GeSn MSM photodetectors

Conventional GeSn MSM photodetectors suffer from a large dark current, which leads to poor signal-to-noise ratio [32–35]. The as-grown GeSn is unintentional p-type doped due to a high concentration of existing vacancies formed during low temperature growth [36,37]. For metal/p-Ge contacts, the Fermi level is pinned at ~0.1 eV above the valence band edge of Ge [38]. Incorporating Sn into Ge shifts up the valence band edge energy [39], which may further decrease the hole Schottky barrier height (ϕ_{bh}), leading to large dark current in GeSn MSM photodetectors. The dark current can be effectively suppressed by increasing ϕ_{bh} (Fermi level de-pinning) through insertion of a large-bandgap material, such as amorphous Si or SiC [40,41], between the metal contact and semiconductor interface. However, the photocurrent was also significantly reduced. It was reported that ϕ_{bh} can be effectively increased by inserting an ultrathin dielectric layer, such AlO_x between the metal and Ge [42]. If the dielectric layer is thin enough, carriers can tunnel through it, while still physically separating the metal from the Ge, and alleviating the Fermi-level pinning.

Figure 3(a) plots the room-temperature current-voltage (I_{dark}-V) characteristics for the fabricated GeSn MSM photodetectors with and without Al_2O_3 interlayer between the metal and Ge. At an applied bias V_{bais} of 1.0 V, high dark current I_{Dark} of ~10 µA was observed in a control photodetector with 2 µm interdigitated fingers, 1 µm spacings and ~10 × 11 µm^2 active areas. A significant dark current suppression by > 2 orders of magnitude can be achieved by inserting an ultrathin Al_2O_3 layer. At V_{bais} of 1.0 V, the I_{Dark} of the GeSn photodetector was measured to be ~65 nA, which is comparable with those of the state-of-the-art GeSn p-i-n photodetectors [43,44]. Based on the thermionic emission model, the I_{Dark} flowing through the MSM photodetector has a strong dependence on temperature T and ϕ_{bh}, and can be described by the following expression

$$I_{dark} = A_p^* T^2 \exp(-\frac{q\varphi_{bh}}{kT}), \quad (1)$$

Optics EXPRESS

where A^*_p is the Richardson's constant for holes, q is the elementary charge, k is the Boltzmann's constant. The I_{Dark} of the GeSn MSM photodetector was characterized at various T ranging from 250 to 350 K with an incremental step of 20 K. Figure 3(b) shows the Arrhenius plot of I_{dark} with and without Al_2O_3 interlayer for the extraction of ϕ_{bh}. Under a constant V_{bias} of 0.5 V, the ϕ_{bh} increased from ~0.12 eV to ~0.32 eV after inserting a 1.5 nm-thick Al_2O_3 layer.

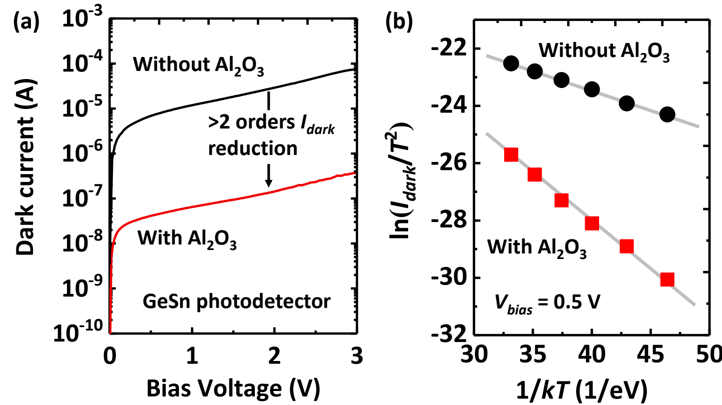

Fig. 3. (a) Dark current was reduced by more than two orders of magnitude by inserting an Al_2O_3 interlayer between Al and Ge. (b) Dark current at various temperatures with and without Al_2O_3 interlayer. The ϕ_{bh} can be effectively increased with an Al_2O_3 interlayer.

3.2 Optical characterization of the GeSn MSM photodetectors

GeSn alloy has smaller bandgap and higher absorption coefficient than those of Germanium (Ge), making it a very promising candidate for photodetection in SWIR range or MIR range [32–35,43–47]. The photoresponse characteristics of the GeSn MSM photodetectors were measured in the wavelength λ range of 1310 – 2003 nm. The light source comprises compact tunable lasers at 1310 – 1350 nm, 1510 – 1630 nm, and three distributed feedback laser diodes at 1742, 1877, and 2003 nm. Figure 4(a) shows the photocurrent I_{photo} of the GeSn MSM photodetector with Al_2O_3 interlayer under illumination at various wavelengths. The active area of the detector with 2 μm interdigitated fingers and 1 μm spacings is 40 × 35 μm^2. As compared to Ge photodetectors, the GeSn MSM photodetector in this work exhibits an extended detection range beyond 2 μm.

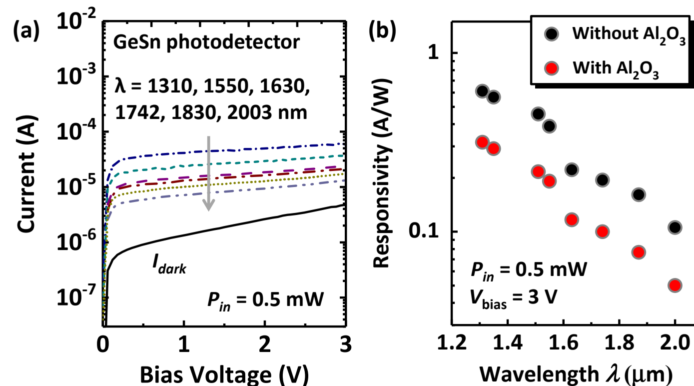

Fig. 4. (a) Photocurrent of the GeSn MSM photodetector with Al_2O_3 interlayer. The arrow points in the direction of increasing wavelengths from 1310 to 2003 nm. (b) Responsivity spectra of GeSn MSM photodetectors with and without Al_2O_3 interlayer.

The responsivity was extracted by taking into account the shadowing of the metal contacts on the top of the GeSn MSM photodetector [Fig. 4(b)]. For the detector without Al_2O_3 interlayer, high responsivities of 0.39 and 0.10 A/W can be observed at 1550 and 2003 nm, respectively. Although the absorption layer is thin, the achieved responsivities at 1550 and 2003 nm is among the highest responsivities reported on GeSn photodetectors [47]. However, while inserting an Al_2O_3 layer, the responsivity was reduced by ~2 times. The responsivity R of the MSM photodetector follows the expression [45]

$$R = G \cdot (\frac{q\lambda}{hc}) \cdot (1-r) \cdot \zeta \cdot [1-\exp(-\alpha_{\lambda} d)], \tag{2}$$

where G is the optical gain, r is the optical power reflectance at the surface, ζ is the fraction of electron-hole pairs that contribute to the detector current, α_λ the absorption coefficient of the material, d the photodetector thickness. The decrease of responsivity may be attributed to two effects. Firstly, the inserted Al_2O_3 layer not only reduces the hole dark current, but may also obstruct the collection of photo-generated carriers (decreasing ζ). Secondly, it should be noted that the photocurrent that is directly generated from the absorption of light is generally magnified by the presence of gain G in MSM photodetector. The ϕ_{bh} is very small for the GeSn MSM photodetector without Al_2O_3 interlayer. If the transit time (t_{tr}) of photogenerated carriers is lower than the lifetime (τ), photoconductor gain (τ/t_{tr}) exists. However, while inserting an Al_2O_3 layer increases ϕ_{bh}, the MSM photodetector works as Schottky diode, which may lead to decreased optical gain. The absorption coefficient α_λ of the strained $Ge_{0.92}Sn_{0.08}$ alloys can be extracted to be ~1920 cm^{-1} at 2003 nm using $\alpha_\lambda = 4\pi k/\lambda$, where k is the extinction coefficient extracted from ellipsometry measurement [48]. Assuming that each absorbed photon generates a single electron-hole pair, and each carrier is collected with 100% efficiency. Without gain, the maximum responsivity at 2003 nm can be calculated to be ~0.03 A/W according to Eq. (2). Since the measured responsivities are higher than this value, the gain exists in the GeSn MSM detectors with and without Al_2O_3 interlayer.

Noise-equivalent power (NEP) is one of the key figures-of-merit of a photodetector, which is often used to quantify the sensitivity of a detector. It is often defined as the signal power that gives a signal-to-noise ratio of one for a bandwidth of 1 Hz. The noise of MSM photodetector mainly consists of four parts: 1/f noise, thermal noise (Johnson noise), and shot noise. The 1/f noise decays as the operating frequency increases, and is not significant for measurement conditions above 1 Hz. Therefore, NEP can be expressed as [49,50]

$$NEP = \frac{\sqrt{(4kT / R_0 + 2qI_{dark})}}{R}, \tag{3}$$

where R_0 is a resistance that can be extracted by taking dV_{bias}/dI_{dark} at 3 V. For the photodetector with and without Al_2O_3 interlayer, the thermal-noise-limited NEP (λ = 1550 nm, V_{bias} = 3 V) can be extracted to be 4.0×10^{-13} and 2.4×10^{-12} $W \cdot Hz^{-1/2}$, respectively, and the dark-current-limited NEP is 1.8×10^{-12} and 1.2×10^{-11} $W \cdot Hz^{-1/2}$, respectively. The NEP is reduced by more than 6 times through inserting an Al_2O_3 layer. The NEP of the GeSn photodetector can be further improved by increasing Sn composition or the thickness of GeSn layer, by implementing the lateral-illuminated (waveguide) structure, or by inserting a barrier layer to reduce the dark current without degradation of the photocurrent. These are subjects for future work.

3.3 Dynamic behavior of the GeSn MSM photodetectors

One main advantage of the MSM photodetector is its low capacitance. It is possible to realize the MSM photodetectors with high responsivity and high speed at the same time. The frequency response of the GeSn MSM photodetector was also investigated. The details of the measurement system are described in [43]. The light source was a fiber-coupled Fabry-Pérot

laser diode (Thorlabs FPL2000S) with λ = 2 μm. The measured 3-dB bandwidth f_{3dB} is 1.4 GHz and 485 MHz for the photodetectors with and without Al_2O_3 interlayer at a V_{bias} of 3 V, respectively (Fig. 5). The active area of the photodetector is 10 × 11 μm^2 with 2 μm interdigitated fingers and 1 μm spacings.

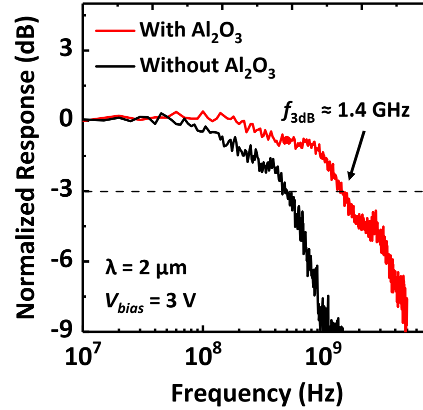

Fig. 5. RF measurement of the GeSn MSM photodetectors with and without Al_2O_3 under illumination at 2 μm. The 3-dB bandwidth of the GeSn MSM photodetector with Al_2O_3 was measured to be 1.4 GHz.

The bandwidth of the MSM photodetectors determined by the transit time and the resistance-capacitance (RC) time constant. Using the conformal mapping approach, the capacitance of the GeSn MSM photodetectors can be simply estimated to be < 10 fF [51]. Then the bandwidth of the GeSn MSM photodetector should not be limited by the RC time constant, but limited by the transit time. It was reported that the background doping (p-type) in as-grown GeSn is high due to low growth temperature growth [36]. The absorption layer cannot be fully depleted at low bias. At high bias, the device is operated in the photoconductive mode, and the bandwidth becomes limited by the lifetime of photogenerated carriers. Here, there is a tradeoff between the optical gain (responsivity) and dynamic behavior of a MSM photodetector. To achieve high response speed, a material with a short carrier lifetime should be used. However, if the carrier lifetime is shorter than the average interelectrode transit time, only a part of the photocarriers will be collected, which tends to decrease responsivity. By tuning the growth technique or growth condition, such as growth temperature, the carrier lifetime in GeSn alloy can be adjusted for various applications.

3.4 Characterization of the GeSn pFinFETs on GeSnOI

As CMOS technologies continuously scale to smaller dimensions, 3D FinFETs have been introduced for advanced technology node beyond 22 nm. To provide better electrostatic control and suppress SCEs, formation of ultrathin fin is needed. GeSn planar MOSFETs on Ge or Ge/Si substrate have been widely investigated due to its higher electron and hole mobilities than that of Ge and Si [8–14]. In this work, GeSn pFinFETs with W_{fin} down to 15 nm were also fabricated on the GeSnOI platform. Figure 6(a) shows the drain current versus gate voltage (I_D-V_G) transfer characteristics of a GeSn pFinFET with channel length L_{ch} of 100 nm, W_{fin} of 15 nm, and H_{fin} of 35 nm. The I_D is normalized by the effective channel width (W_{eff}) which is equal to (2 × H_{fin} + W_{fin}). This device shows S of 93 mV/decade and on-state drain current/off-state leakage current (I_{ON}/I_{OFF}) ratio of more than 4 orders at V_{DS} of –0.05 V. A very low gate leakage current (I_G) of ~8 × 10^{-5} μA/μm at the gate bias (V_G) of −1.2 V is maintained. Small drain-induced barrier lowering (DIBL) of 33 mV/V was obtained, indicating good SCEs control. The I_D-V_{DS} output characteristics of the same device are shown in Fig. 6(b). The gate-over-drive (V_G − V_{TH}) was varied from 0 to −1 V in steps of –0.1 V.

Optics EXPRESS

Good saturation behavior is observed, with I_D of 176 μA/μm at ($V_G - V_{TH}$) of −1.0 V and V_{DS} of −1.2 V. Another device with L_{ch} of 100 nm and W_{fin} of 100 nm was also fabricated. The DIBL significantly increases to more than 200 mV/V, due to poor electrostatic control over the channel with large W_{fin}.

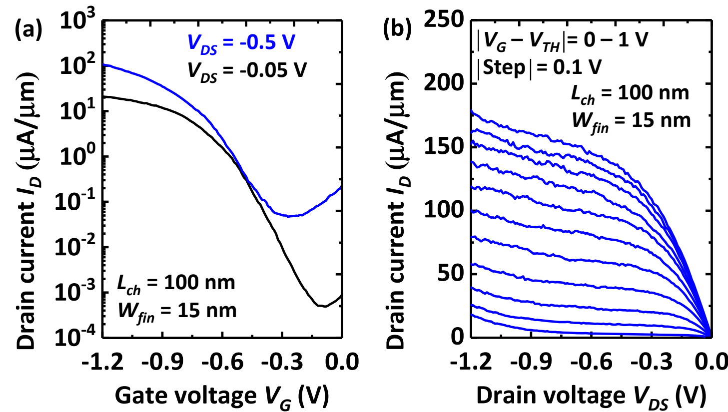

Fig. 6. (a) I_D-V_G of a GeSn pFinFET with W_{fin} of 15 nm and L_{ch} of 100 nm that exhibits S of 93 mV/decade at V_{DS} of −0.05 V. (b) I_D-V_{DS} of the same device in (a) shows a drive current of 176 μA/μm at $|V_G$-$V_{TH}|$ of 1 V and V_{DS} of −1.2 V.

4. Summary

GeSn MSM photodetectors were realized on a GeSnOI platform with detection range extends beyond 2003 nm. High responsivities of 0.39 and 0.10 A/W were achieved at 1550 and 2003 nm, respectively. An Al_2O_3 interfacial layer was used to increase the Schottky barrier at metal and semiconductor interface, leading to significant dark-current I_{Dark} suppression by more than two orders of magnitude. Low I_{Dark} of ~65 nA was achieved at V_{bias} of 1.0 V, which is comparable to that of the state-of-the-art GeSn photodetectors. The dynamic behavior of the photodetector was also investigated. A 3-dB bandwidth of 1.4 GHz was achieved at 2 μm for the photodetector with the Al_2O_3 interfacial layer. GeSn pFinFETs were also fabricated on the GeSnOI platform with W_{fin} down to 15 nm. Good electrical characteristics were achieved, with small subthreshold swing of 93 mV/decade, high drive current of 176 μA/μm, and good control of SCEs. This work opens up the possibility for monolithic integration of high-performance GeSn electronic and photonic devices on insulators.

Funding

National University of Singapore Trailblazer (Grant No. R-263-000-B43-733) and Ministry of Education (MOE) Academic Research Fund (Grant No. R-263-000-B50-112).

Acknowledgments

We thank Dr. Xin Guo at Silicon Technologies, Centre of Excellence (Si-COE) in Nanyang Technological University for the RF measurement of the photodetectors, and thank Dr. Zhihong Liu and Dr. Chongyang Liu for technical discussions on the RF measurement.

155.69.3.156 {ts '2019-01-31 01:24:05'}